BIOCHEMISTRY
including biophysical chemistry & molecular biology

ARTICLE

pubs.acs.org/biochemistry

Structural Characterization of Three Novel Hydroxamate-Based Zinc Chelating Inhibitors of the *Clostridium botulinum* Serotype A Neurotoxin Light Chain Metalloprotease Reveals a Compact Binding Site Resulting from 60/70 Loop Flexibility

Aaron A. Thompson,[†] Guan-Sheng Jiao,[‡] Seongjin Kim,[‡] April Thai,[‡] Lynne Cregar-Hernandez,[§] Stephen A. Margosiak,[§] Alan T. Johnson,[‡] Gye Won Han,[†] Sean O'Malley,[‡] and Raymond C. Stevens*[,†]

[†]Department of Molecular Biology, The Scripps Research Institute, La Jolla, California 92037, United States

[‡]Department of Chemistry, PanThera Biopharma LLC, Aiea, Hawaii 96701, United States

[§]Department of Lead Discovery, PanThera Biopharma LLC, Aiea, Hawaii 96701, United States

Supporting Information

ABSTRACT: Neurotoxins synthesized by *Clostridium botulinum* bacteria (BoNT), the etiological agent of human botulism, are extremely toxic proteins making them high-risk agents for bioterrorism. Small molecule inhibitor development has been focused on the light chain zinc-dependent metalloprotease domain of the neurotoxin, an effort that has been hampered by its relatively flexible active site. Developed in concert with structure−activity relationship studies, the X-ray crystal structures of the complex of BoNT serotype A light chain (BoNT/A LC) with three different micromolar-potency hydroxamate-based inhibitors are reported here. Comparison with an unliganded BoNT/A LC structure reveals significant changes in the active site as a result of binding by the unique inhibitor scaffolds. The 60/70 loop at the opening of the active site pocket undergoes the largest conformational change, presumably through an induced-fit mechanism, resulting in the most compact catalytic pocket observed in all known BoNT/A LC structures.

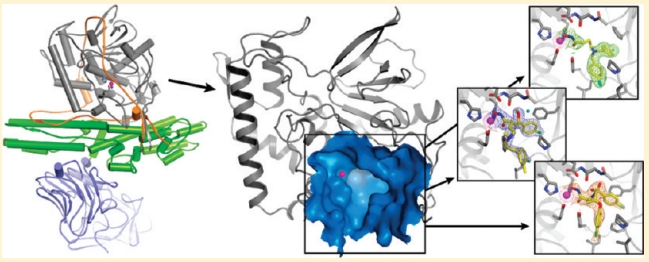

Neurotoxins synthesized by the anaerobic bacterium *Clostridium botulinum*, the causative agent of botulism, are categorized into seven distinct serotypes based on immunogenic properties (A−G). These toxins typically enter peripheral cholinergic neurons where they inhibit release of the neurotransmitter acetylcholine by preventing docking of the synaptic vesicle with the presynaptic membrane, ultimately resulting in flaccid muscle paralysis of the host. Human botulism is caused by *C. botulinum* neurotoxin (BoNT) serotypes A, B, E, and F, with the most potent of these, type A (BoNT/A), displaying a lethal dose of only 1 ng/kg of body weight.[1,2] Besides causing naturally occurring botulism, BoNT is also classified by the Centers for Disease Control and Prevention as a Category A agent, making it one of the highest-risk threat agents for bioterrorism (http://emergency.cdc.gov/agent/agentlist-category.asp). Current treatment regimens rely on antibody-based antitoxins that cannot interact with the toxin once it has entered the neuron, where the activity of the BoNT/A light chain can persist for months (reviewed in ref 3). The development of small molecule inhibitors as intraneuronal therapeutics is a crucial unmet need.

The crystal structure of BoNT shows three functional domains comprised of an ∼50 kDa light chain (LC) and a heavy chain (HC) containing two segments that are each approximately ∼50 kDa (Figure 1A,B).[4] The C-terminal portion of the HC is the cell binding domain and is responsible for docking the toxin to gangliosides and a protein receptor(s) on presynaptic neurons resulting in toxin endocytosis. The translocation domain, at the N-terminal portion of the HC, mediates escape of the toxin LC from the endosome into the neuronal cytosol. The LC is a zinc-dependent endopeptidase that is involved in serotype-dependent cleavage of one or more members of the soluble *N*-ethylmaleimide sensitive factor attachment protein receptor (SNARE) complex of proteins involved in synaptic vesicle docking. BoNT/A specifically cleaves between residues Gln197 and Arg198 of the 206-residue SNAP-25 protein (synaptosome-associated protein of 25 kDa). A unique feature of BoNT LCs is their requirement for relatively long substrates when compared to other zinc-dependent endopeptidases outside of the clostridial family. BoNT/A LC requires a minimal SNAP-25 peptide sequence of ∼51 amino acids to achieve efficient cleavage, and optimal binding occurs with only full-length SNAP-25.[5,6] The crystal structure of SNAP-25$_{141-204}$ (residues 141−204) bound to BoNT/A LC (residues 2−420 with E224Q and Y366F active site

Received: January 28, 2011
Revised: March 23, 2011
Published: March 24, 2011

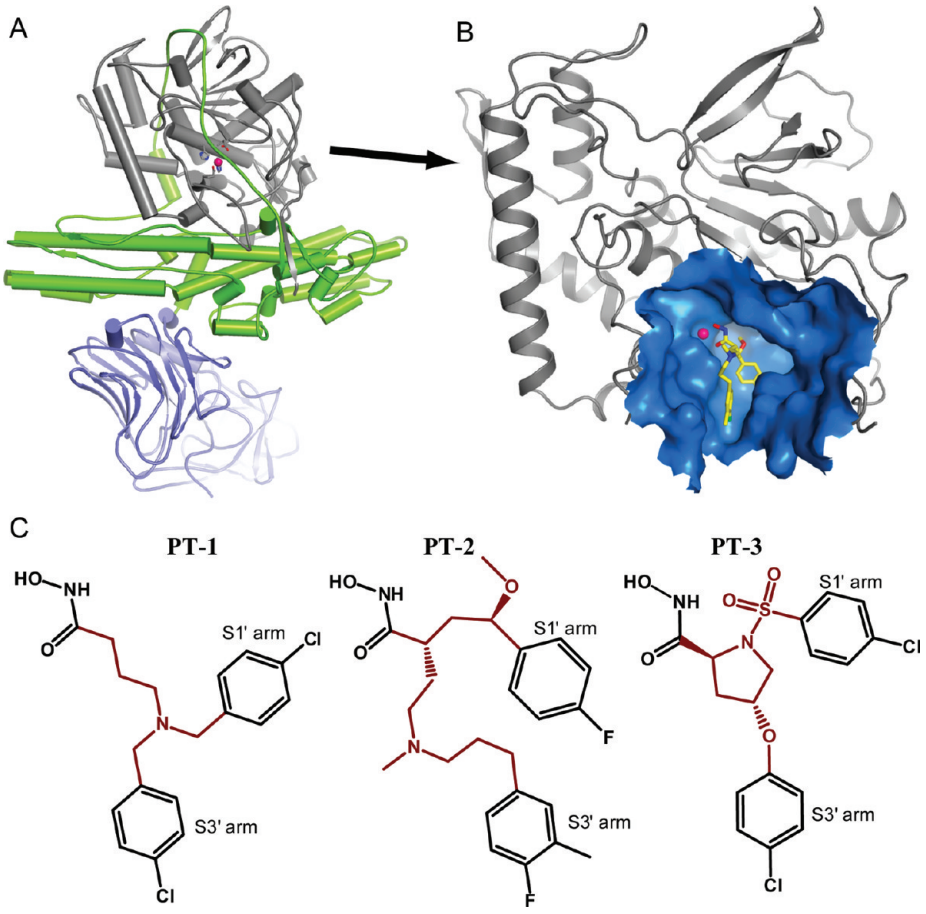

Figure 1. Overview of BoNT/A, LC, and the chemical structures of the inhibitors used in this study. (A) BoNT/A holotoxin structure from PDB entry 3BTA[4] with the LC colored gray and the HC's translocation and cell binding domains colored green and blue, respectively. (B) BoNT/A LC domain colored gray with a surface representation of the active site pocket colored blue. PT-2 (yellow sticks) is complexed with the LC deep within the active site pocket. (C) Each inhibitor contains a unique scarlet-colored scaffold that bridges a zinc chelating hydroxamate moiety located on the left of each chemical structure and halogenated benzene-containing arms (S1′ and S3′ arms).

mutations) provides an explanation for this finding as binding involves protein exosites that anchor the substrate and position the scissile bond for cleavage.[7] Binding of SNAREs to protein exosites flanking the active site pocket likely influences the high degree of substrate specificity because of the decrease in entropy that allows the scissile bond to orient into the deep active site via a sharp stereochemically strained conformation (Figure S1A,B of the Supporting Information). Insight into SNAP-25−BoNT/A LC subsite interactions was revealed by the BoNT/A LC structure (native active site) in a complex with a smaller SNAP-$25_{197-202}$ peptide fragment (residues 197−202).[8] Catalysis occurs within a relatively deep active site pocket measuring ~22 Å × ~22 Å × ~25 Å. Cleavage by LCs of substrate SNARE proteins does not allow for the formation of ternary complexes that are believed to drive synaptic vesicle fusion and exocytosis of neurotransmitters (reviewed in refs 9−13).

The clostridial neurotoxin LCs are zinc-dependent endopeptidases representing a unique family of zinc metalloproteases in the gluzincin superfamily, with thermolysin being the prototypical member. The primary sequences of thermolysin and the BoNT LCs contain a conserved HEXXH motif that is required for chelation of a catalytic zinc ion and a putative interaction with a water molecule thought to be involved in the general base mechanism of catalysis.[4,7] While a structure-based homology server (Dali[14]) search suggests thermolysin is currently the closest structural neighbor to clostridial LCs, comparison of the solvent accessible surface of the active site pockets reveals significant differences in the shape and volume of these pockets (Figure S1 of the Supporting Information). In the serotype A LC, His223 and His227 from the HEXXH motif are involved in binding zinc along with a conserved Glu262 that is located approximately 30 amino acids downstream of the motif (Figure S1E,F of the Supporting Information). The Glu224 from this conserved HEXXH motif is believed to act as a general base by polarizing a water molecule, thereby preparing it for nucleophilic attack of the scissile peptide bond's carbonyl carbon atom. The primary sphere of residues coordinating the catalytic zinc is identical among clostridial neurotoxin LCs and other members of the gluzincin family, such as the prototypical thermolysin protease; however, there are potentially significant differences in the secondary sphere of residues that can be attributed to diversity in substrate preference. Differences include Arg363 and Tyr366 of BoNT/A LC that are thought to stabilize the nascent oxyanion formed during the proteolytic cleavage event, residues lining the S1, S1′, S2′, and S3′ binding pockets, and the surface area of active site pockets (Figure S1 of the Supporting Information). These differences from other gluzincin proteases suggest that development of inhibitors selective for zinc-dependent endopeptidases from the *Clostridium* family is possible.

There are several reports of small molecule inhibitors of BoNT/A LC. Most of these inhibitors bear a zinc binding group, either a hydroxamic acid,[15,16] a thioacetyl group,[17] or a hydroxyquinoline group;[18] a subset are highly positively charged but lack a clear zinc binding group.[19] PanThera Biopharma LLC has embarked on a program to develop postexposure intraneuronal therapeutics for BoNT/A intoxication through the optimization of hydroxamic acid inhibitors; multiple distinct structural series are currently being investigated. In this study, we present the X-ray crystal structures of inhibitors representing three distinct, branched scaffolds and discuss significant interactions between the inhibitors and their BoNT/A LC target, focusing on the key 60/70 loop (BoNT/A LC residues 60−79) movement that appears to be critically important for understanding the binding of these inhibitors.

EXPERIMENTAL PROCEDURES

Cloning, Expression, and Purification of BoNT/A LC. The cDNA encoding a 424-amino acid gene for the BoNT/A LC protease was synthesized by DNA2.0 with codon optimization for expression in *Escherichia coli* and then cloned into inducible T7-based expression vector pET23a (Novagen). After being expressed in *E. coli* BL-21(DE3)pLysS, the cells were resuspended in 20 mM TRIS (pH 8.0), 300 mM NaCl, and 10 mM imidazole (pH 8.0) and lysed using a cell disruptor (Microfluidics). The lysate was centrifuged at 20000*g*, and the supernatant was filtered with a 0.2 μm cutoff syringe filter. The lysate was then transferred to a gravity column containing a 5 mL bed volume of IMAC Sepharose 6 FF (GE Healthcare) charged with $ZnCl_2$ and equilibrated with lysis buffer and eluted with a linear gradient from 10 to 400 mM imidazole in 20 mM TRIS (pH 8.0) and 300 mM NaCl. Fractions containing BoNT/A LC were pooled, and ammonium sulfate was added to a final concentration of 0.8 M. This protein was loaded onto a 5 mL Butyl-FF column (GE healthcare) and eluted using a linear gradient from 0.8 to 0.1 M ammonium sulfate in 50 mM HEPES (pH 7.5). The fractions containing BoNT/A LC were again pooled and concentrated using Amicon Ultra-4 30K molecular weight cutoff centrifugal filtration devices (Millipore) and then run over a Superdex 200 column equilibrated in 200 mM NaCl and 10 mM HEPES (pH 7.5). The purified protein was concentrated to ∼15 mg/mL for crystallization.

BoNT/A LC Proteolytic Assay. A fluorescence resonance energy transfer (FRET) assay was used to determine the inhibition kinetics and K_i values of BoNT/A LC inhibitors using Abz-TdRIDEANQRATKnLK(dnp)-NH_2 as the peptide substrate. Cleavage was assessed as an increase in fluorescence with a λ_{ex} of 320 nm and a λ_{em} of 420 nm. The 100 μL reaction mixture contained 13 nM BoNT/A LC_{1-429} in 30 mM HEPES (pH 7.3), 0.05 mM zinc acetate, 0.05% Tween 20, 0.1 mg/mL BSA, 2.5% DMSO, and 25 μM peptide substrate. The reaction was initiated with addition of substrate and the mixture incubated for 10 min (23 °C) while the increase in fluorescence was measured to obtain a steady state rate of product formation. Steady state rates were used to determine K_i values by fitting to the classical competitive inhibition equation.

Crystallization and Structure Determination. Crystals are grown by sitting nanodrop vapor diffusion at 20 °C using an ∼7−10 mg/mL protein sample, 0.5 mM inhibitor compound when applicable, and the Innovadyne Screenmaker crystallization robot. Zinc-bound BoNT/A LC and the PanThera compound 2 (PT-2) (Figure 1C) BoNT/A LC complex belonging to space groups $P2_1$ and $P2_12_12$, respectively, grew in ∼10 days from 5% glycerol and 15% PEG 6000, with glycerol added to a final concentration of 20% for cryoprotection. The PanThera compound 3 (PT-3) (Figure 1C) BoNT/A LC complex crystals grew in ∼30 days with a precipitant/well solution containing 10% PEG 6000 and 100 mM MES (pH 6.5), and the PanThera compound 1 (PT-1) (Figure 1C) BoNT/A LC complex crystals grew in ∼30 days with a precipitant/well solution containing 13% PEG 6000 and 100 mM MES (pH 6.9). Ethylene glycol was briefly added to a final concentration of 20% for cryoprotection. Diffraction data were collected at Advanced Light Source beamlines 12.3.1 and 4.2.2 (Berkeley, CA) and SSRL beamline 11.1 (Palo Alto, CA). Reflections were processed using HKL2000,[20] and the initial structure solution was obtained by molecular replacement with Phaser[21] using BoNT/A LC (PDB entry 3DDA[8]) as the search model. The PT-1 complexed crystals displayed anisotropic diffraction; a complete data set was obtained by merging data collected from two crystals. Manual model rebuilding was performed using Coot[22] and refined with the Phenix software suite,[23] and the PT-1 structure was refined further using autoBUSTER.[24] TLS refinement was used at the final stages of refinement with one to three TLS domains defined per protease molecule.[25] Figures were generated with Pymol Molecular Graphics System version 1.0r2, and structure-based alignments were performed using Pymol's "super" algorithm (http://www.pymol.org). Data and refinement statistics are listed in Table 1.

Coordinates and Structure Factors. The coordinates and structure factors have been deposited in the RCSB Protein Data Bank as entries 3QIX (unliganded), 3QIY (PT-1 complex), 3QIZ (PT-2 complex), and 3QJ0 (PT-3 complex).

Inhibitor Synthesis. Synthesis of the inhibitors will be described elsewhere (manuscripts in preparation). PT-2 was prepared according to previously reported methods for structurally related anthrax lethal factor inhibitors.[26]

RESULTS

BoNT/A LC Structures Bound with Zinc. Using a construct consisting of the first 424 residues of BoNT/A LC, we obtained the structure of its ligand-free zinc-bound form with crystals belonging to space group $P2_1$. This crystal structure contained two molecules in the asymmetric unit; the individual molecules were not significantly different from each other with a C_α rmsd of 0.38 Å. Several loops located in the proximity of the large active site opening, the 250 and 190 loops, display relatively weak or absent electron density in both LC molecules, suggesting flexibility in this region. Electron density for a single zinc ion was observed in each catalytic site coordinated by His223, His227, and Glu262, and a water molecule with weak density is present in the absence of an inhibitor (Figure S2 of the Supporting Information).

The three inhibitors used in this study are shown in Figure 1C. Each contains three binding moieties, two halogenated phenyl rings and a zinc-binding hydroxamate group, which are connected via three different branched scaffolds. Each ring lies at the end of a flexible arm with one arm binding to the S1′ site (here termed the S1′ arm) and the other to the S2′ and S3′ sites (here termed the S3′ arm). These inhibitors display K_i values in the single-digit micromolar range (Table 2). Despite the presence of relatively large solvent channels leading to the active site pockets, crystallization of BoNT/A LC in complexes with each of the three inhibitors required cocrystallization; attempts to soak them into the $P2_1$ BoNT/A LC crystals were unsuccessful (Table 1).

Table 1. Summary of Crystallographic and Structure Refinement Data

	unliganded	PT-1	PT-2	PT-3
PDB entry	3QIX	3QIY	3QIZ	3QJ0
space group	$P2_1$	$P2_12_12$	$P2_12_12$	$P2_12_12$
no. of protomers/atoms per asymmetric unit	2/6501	1/3241	1/3430	1/3309
unit cell dimensions	a = 38.8 Å	a = 59.1 Å	a = 59.2 Å	a = 59.2 Å
	b = 193.7 Å	b = 190.6 Å	b = 190.7 Å	b = 188.8 Å
	c = 56.0 Å	c = 42.7 Å	c = 42.3 Å	c = 42.6 Å
	β = 96.1°			
X-ray source	ALS 12.3.1	SSRL 11.1	SSRL 11.1	SSRL 11.1
		Reflections		
resolution limits (Å)	50−2.4 (2.49−2.4)[a]	45−2.3 (2.38−2.3)[a]	45−2.0 (2.07−2.0)[a]	45−2.3 (2.38−2.3)[a]
total no. of reflections collected	333387	713428	619655	860557
no. of unique reflections	31317	20556	30442	20915
redundancy	3.8 (3.7)[a]	13.4 (10.5)[a]	6.8 (4.6)[a]	13.74 (11.9)[a]
$\langle I\rangle/\langle\sigma(I)\rangle$	13.9 (2.6)[a]	10.8 (4.7)[a]	16.7 (2.5)[a]	29.3 (16.9)[a]
completeness (%)	100 (99.9)[a]	91.6 (80.7)[a]	90.8 (79.2)[a]	94.6 (95.4)[a]
R_{merge} (%)	9.3 (47.8)[a]	9.6 (32.8)[a,b]	8.8 (48.8)[a]	5.8 (28.7)[a]
		Refinement		
resolution range (Å)	50−2.4	45−2.3	45−2.3	45−2.3
R_{work} (%)	18.5	22.6	18.8	19.8
R_{free} (%)	22.8	26.4	22.3	22.9
rmsd for bond lengths (Å)	0.012	0.009	0.01	0.01
rmsd for bond angles (deg)	1.4	1.08	1.27	1.09
mean B factor (Å^2)				
protein atoms	44.5	88.0	49.6	69.2
inhibitor/zinc	NA/86.4	91.0/57.5	48.3/31.2	71.9/48.7
water	38.0	68.5	45.7	57.0

[a] Data in parentheses are for the highest-resolution shell. [b] The PT-1 data set is merged from data collected on two crystals.

Interestingly, the inhibitor-bound structures crystallized in a different space group, $P2_12_12$, with significantly different cell dimensions. The ligand binding sites for the three inhibitor complexes in these crystal structures are shown in Figure 2 and Figure S2 of the Supporting Information.

Ligand-Binding Conformational Changes Indicate Possible Induced Fit. The inhibitor-bound structures confirm that the hydroxamate moiety is engaged in a planar bidentate interaction with the catalytic zinc (Figure 2). The hydroxamate groups appear to be locked in place by hydrogen bonding interactions with the backbone carbonyl of Phe163, and the catalytically important residues Glu224 and Tyr366 (Figure 2). The latter is believed to play a role in the stabilization of the oxyanion formed during native substrate cleavage. While the arms of these inhibitors have been designed to exploit the relatively hydrophobic nature of the active site pocket, the scaffolds used in PT-2 and -3 have additional groups that facilitate potential hydrogen bonding with the "roof" of the catalytic pocket. PT-2 contains a methoxy group that interacts with the backbone of residues 161 and 163 through a water-mediated hydrogen bond, while the sulfur dioxide group of PT-3 interacts directly with the backbone nitrogen of residue 163. A structure-based superposition of the BoNT/A LC structures that down-weights amino acid pairings with high relative variability has revealed multiple conformational changes that are presumably a consequence of inhibitor binding (Figure 3). The most significant differences occur around Phe194, the 360/370 loop (residues 366−372), and the 60/70 loop (residues 61−79).

Table 2. Inhibition Constants for the Inhibitors against BoNT/A LC

inhibitor	K_i (μM) ± standard deviation
PT-1	4.6 ± 1.8
PT-2	6.1 ± 2.5
PT-3	6.3 ± 0.89

Phe194 Can Assume a Different Rotamer upon Ligand Binding. Aromatic groups from the S1′ arm of the inhibitors exploit the deep cavity of the S1′ subsite of the binding pocket that in the SNAP-25$_{197-202}$ peptide-bound structure[8] is formed by Phe194 and Asp370. Phe194 appears to be poised to facilitate cation−π stacking interactions with the guanidinium group of the SNAP-25 P1′ arginine residue, and Asp370 forms the "floor" of the S1′ subsite via formation of a salt bridge with the P1′ arginine (Figure S3 of the Supporting Information). The positioning of Phe194 and Asp370 from the SNAP-25$_{197-202}$-bound structures is almost identical to that of the BoNT/A holotoxin structures (PDB entries 3BTA, 2NYY, and 2NZ9), suggesting these residues are prepositioned for optimal interaction with the P1′ residue. This is supported by the fact that Phe194 and Asp370 are also prepositioned in almost all previously published apo and zinc-loaded BoNT/A LC structures (PDB entries 1XTF, 2IMC, 2ISE, 2ISH, 2W2D, 3BOK, 3BON, and 3BWI). Surprisingly, Phe194 from the zinc-bound $P2_1$ structure presented in this study is observed in the p90 rotamer configuration (rotamers described in ref 27), and

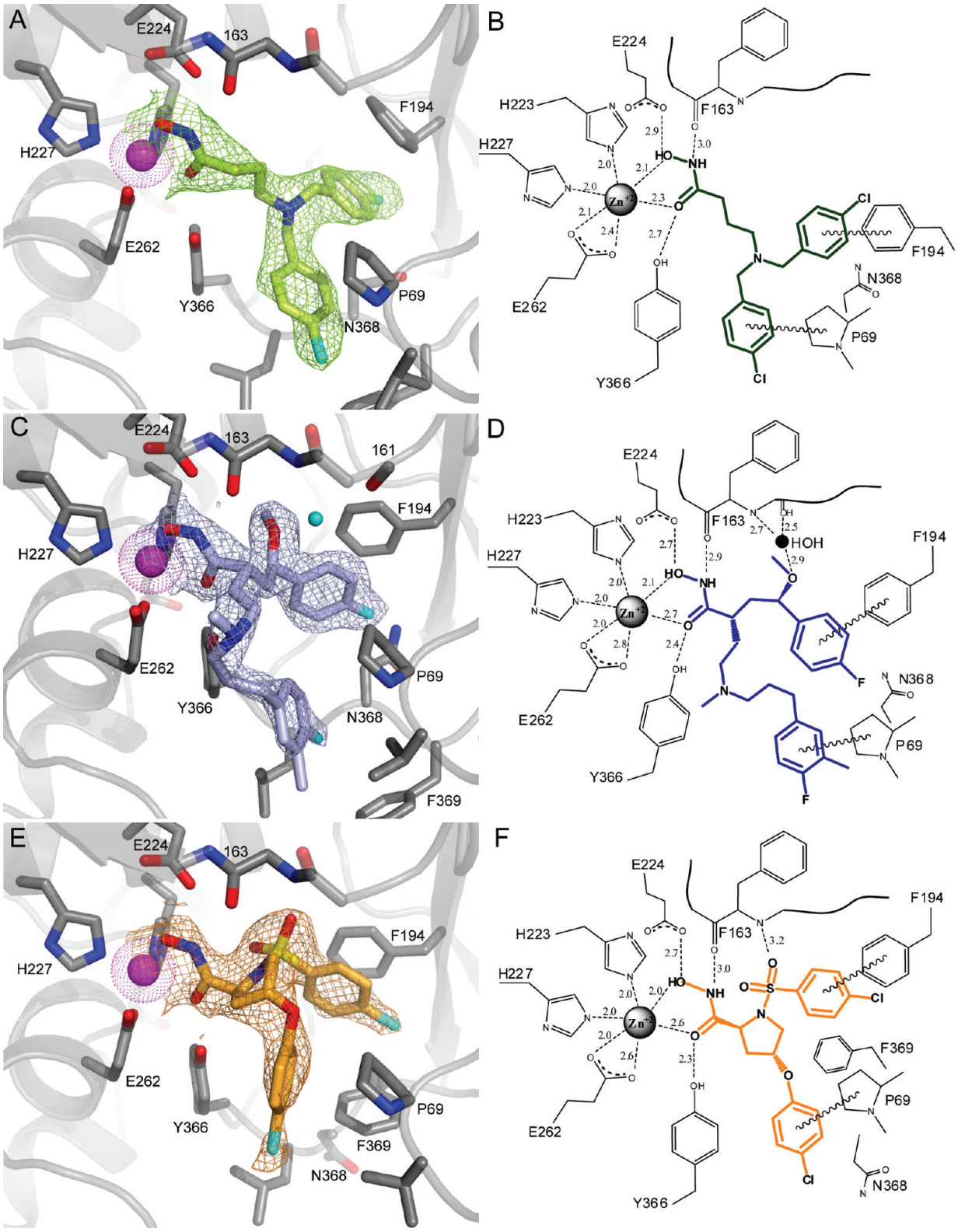

Figure 2. Structures and schematics of BoNT/A LC bound by hydroxamate inhibitors. 1500K SA-OMIT $2|F_o| - |F_c|$ electron density maps contoured at 1.5σ around the hydroxamate inhibitors (carve = 1.7 Å) with the zinc ion depicted as a magenta sphere, alongside schematic representations of the enzyme−inhibitor complexes of (A and B) PT-1, (C and D) PT-2, and (E and F) PT-3. The schematic shows potential hydrogen bonds represented as dashed lines and hydrophobic $\pi-\pi$ stacking interactions as wavy lines.

Asp370 from a separate zinc-bound LC structure (PDB entry 2ISG) is pointed "out" and away from the catalytic center, thereby alluding to the structural plasticity of the active site pocket (Table 3 and Figure S2 of the Supporting Information).

dx.doi.org/10.1021/bi2001483 |*Biochemistry* 2011, 50, 4019–4028

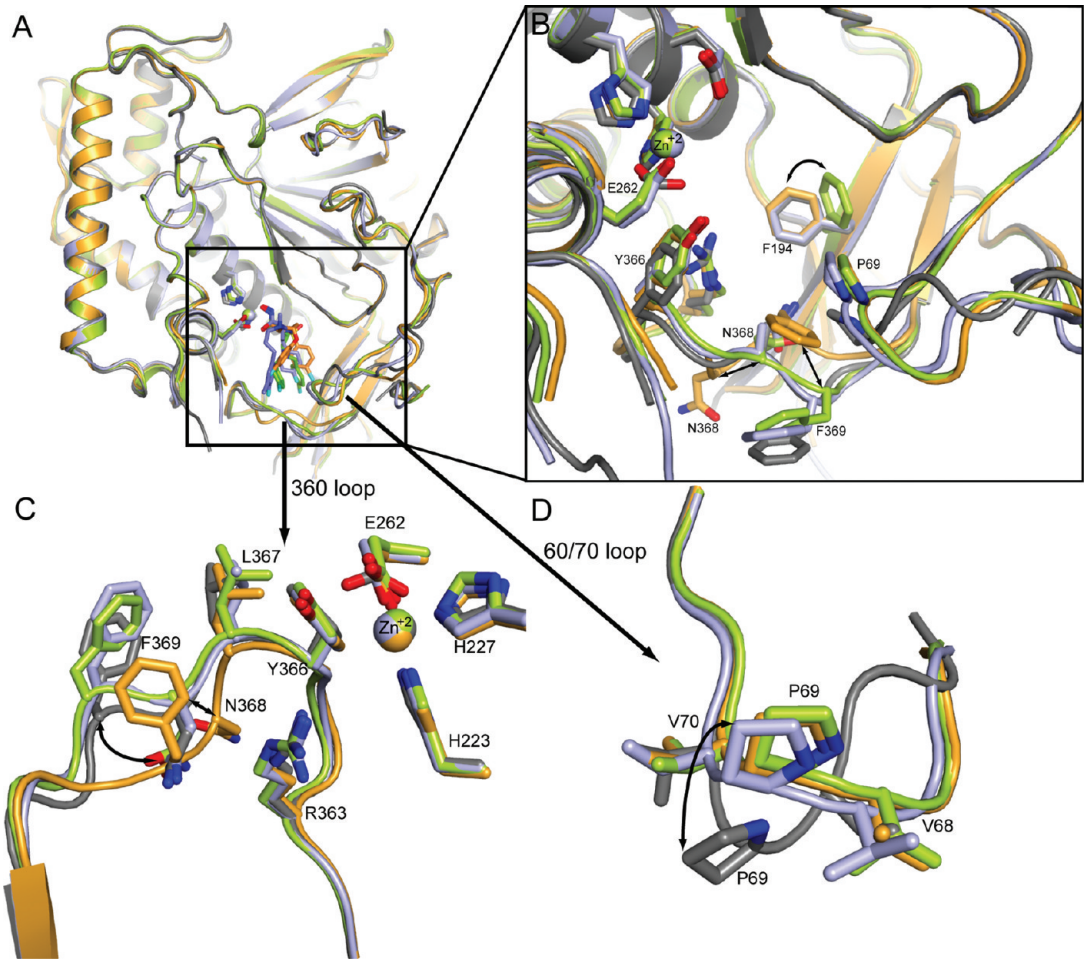

Figure 3. Induced conformational changes around the active site of BoNT/A LC. (A) Structure-based alignment of unliganded BoNT/A LC (chain A, gray) and LC complexed with PT-1 (green), PT-2 (blue), and PT-3 (orange). (B) Close-up of the active site with the inhibitors omitted to highlight the structural changes observed around the binding site. (C) Close-up of the 360 loop viewed from the center of the active site. (D) Close-up of the 60/70 loop viewed from the center of the active site.

The S1′ arms of the inhibitor structures all reveal hydrophobic stacking against the side chain of Phe194, which is allowed by assuming alternate side chain rotamer conformations with negligible deviations from the backbone (Figure 3B). Residue Phe194 from the PT-1-bound BoNT/A LC structure adopts the m-85 rotamer conformation similar to the holotoxin, and SNAP-25- and most apo/zinc-bound BoNT/A LC structures. Phe194's side chain conformations in the structures of the PT-2 and -3 complexes are rotated to the less commonly observed p90 rotamer, optimizing the π-stacking interactions with these inhibitors (Figures 2 and 3B and Figure S2 of the Supporting Information). When compared with a random PDB data set containing 1570 occurrences of Phe at 1.7 Å resolution or higher, 44% of the structures adopt the m-85 rotamer versus 13% of the structures adpoting the p90 rotamer.[27]

Conformational Changes to the 360/370 Loop upon Ligand Binding: Asn368 or Phe369 Can Replace Asp370 in Forming the S1′ Subsite. The conformational flexibility of this domain has been previously described with small molecule[28] and peptidyl ligands.[29] Interactions between the inhibitor hydroxamate group's carbonyl oxygen and the exocyclic hydroxyl group of Tyr366, in combination with hydrophobic and van der Waals forces between the S3′ arms of the compounds, appear to "pull" this amino acid residue into the active site, thereby altering the positioning of the 360 loop (Figure 3B,C). Binding by PT-3 results in the most dramatic changes in this loop, with residues Asn368 and Phe369 showing significant deviations from their positions in the zinc-bound BoNT/A LC; the C_α atom of Asn368 is displaced by 3.0 Å with its side chain pointed away from the catalytic center, and the C_α atom of Phe369 is displaced by 4.2 Å toward the active site (Figure 3B,C). While Asp370 in the SNAP-$25_{197-202}$ and most other peptide-bound structures was observed to be a key residue of the S1′ subsite,[8,29−31] it is pointed away from the catalytic center in the presented structures, thereby creating a large pocket between residues Phe194 and Pro69 that accommodates the aromatic arm substituents. Interestingly, Phe369 from the PT-3 structure (but not from the PT-1 or PT-2 structures) is positioned to fill the void from the displaced Asp370, creating a hydrophobic floor for the S1′ subsite. Similar reconfigurations in the S1′ subsite were observed with the hydrophobic chlorocinnamic hydroxamate inhibitors (PDB entries 2IMA and 2ILP[28]). However, in the PT-1 and PT-2 structures, it is residue Asn368 that replaces Asp370 to create one wall of the S1′ subsite; this feature is unique to these inhibitor complexes and has not previously been reported.

Conformational Changes to the 60/70 Loop upon Ligand Binding. Structure-based alignment of the structures in this

dx.doi.org/10.1021/bi2001483 |*Biochemistry* 2011, 50, 4019–4028

Table 3. Conformational Changes within the BoNT/A LC Active Site Pocket

structures	distance[a] from Pro69 to Zn^{2+} (Å)	Phe194 rotamer[b]	Asn368	Phe369	Asp370
LC and PT-1 (3QIY)	12.5	m-85	in	out	out
LC and PT-2 (3QIZ)	12.6	p90	in	out	out
LC and PT-3 (3QJ0)	11.8	p90	out	in	out
LC[c] and zinc (3QIX)	14.6	p90	in	out	out
LC[c] and zinc (2ISG)	17.3	m-85	in	out	out
LC,[c] zinc, and His tag[c] (1XTF)	18.7	m-85	out	out	in
LC and zinc (2IMC)	18.1	m-85	out	out	in
LC[c] and zinc[c] (2ISE)	18.1	m-85	out	out	in
LC[c] and zinc[c] (2ISH)	18.6	m-85	out	out	in
LC[c] and zinc[c] (2W2D)	14.6	m-85	out	out	in
apo LC (3BOK)	not available	m-85	out	out	in
LC and zinc (3BON)	17.6	m-30/m-85	out	out	in
LC and zinc (3BWI)	18.3	m-85	out	out	in
LC and $SNAP25_{141-204}$ (1XTG)	15.2	m-85	out	out	in
LC and $SNAP25_{197-202}$ (3DDA)	18.2	m-85	out	out	in
LC[c] and hydroxamate inhibitor (2IMA)	15.2	p90	out	in	out
LC[c] and hydroxamate inhibitor (2IMB)	18.9	m-85	out	out	in
LC and CRATKML (3BOO)	17.4	m-85	out	out	in
holotoxin (3BTA)	15.2	m-85	out	out	in
holotoxin and mAb (2NYY)	15.4	m-85	out	out	in
holotoxin[c] and mAb (2NZ9)	15.3	m-85	out	out	in

[a] Distances are between the C_α atom of Pro69 and the Zn^{2+} from each respective structure. [b] Rotamers defined by Lovell et al.[26] [c] Data for the structure with LC and zinc refer to monomer A.

study indicated that the largest conformational changes are primarily situated around the opening of the active site pocket (Figure 3). The 60/70 loops (residues 60−79) show the most consistent change in conformation resulting from hydrophobic interactions between Pro69 of BoNT/A LC and aromatic moieties on the S3′ arm of the compounds. The Pro69 C_α positions of the inhibitor-complexed BoNT/A LC structures are pulled between 2.85 and 3.1 Å into the active site when compared to those of the uncomplexed protease (Figure 3D). These structures represent the most compact conformations of the 60/70 loop yet reported; the difference in the distance from the active site zinc atom to the Pro69 C_α atom ranges from a minimum of 2.6 Å for the nearest reported compact structure [cf. PT-2 to 1XTG (Table 3)] to 7.1 Å for the most "open" structure reported [cf. PT-3 to 2IMB (Table 3)]. The 60/70 loop conformations of the zinc- and inhibitor-bound structures presented in this study are very different from those of the $SNAP\text{-}25_{197-202}$ peptide-bound structure (PDB entry 3DDA), most likely because of the presence of the bulkier peptidyl ligand in the active site (Figure S3 of the Supporting Information). To accommodate the P4′ and P5′ residues of SNAP-25, this loop is pushed away from the catalytic center, resulting in Pro69 C_α displacements on the order of 6−7 Å (Table 3). Pro69 from the BoNT/A LC structure bound with the longer $SNAP\text{-}25_{146-204}$ peptide (PDB entry 1XTG) is in a conformation similar to that of our $P2_1$ zinc-bound BoNT/A LC structure with a C_α difference of ∼1.2 Å,[7] although this is possibly due to the presence of active site mutations in the $SNAP\text{-}25_{146-204}$-bound BoNT/A LC structure that preclude native substrate−active site interactions.

Structural Comparisons with Previously Reported Hydroxamate Inhibitors. Small (∼190−230 Da) "rodlike" zinc chelating hydroxamate inhibitors have previously been characterized by X-ray crystallography.[28] These inhibitors are hydroxamic acid derivatives bearing either a single L-arginine arm or a 2,4-dichlorocinnamate aromatic arm that occupies the S1′ subsite similar to the S1′ arm of the inhibitors described in this study (Figure 4). We observe induced-fit changes in the active site pocket residues that accommodate the inhibitors that are similar to those seen in the Silvaggi study in one case (PT-3); in the other two structures, there are key differences in the role of Asn368 in the formation of the S1′ subsite. The conformation of Phe194 from the L-arginine hydroxamate structure (PDB entry 2IMB) is similar to that found in the PT-1 structure, whereas Phe194 from the chlorocinnamic hydroxamate structures (PDB entries 2IMA and 2ILP) is similar to that of the PT-2 and -3 structures (Figure 4). In the PT-3 structure, Phe369 is pulled up into the active site to form a portion of the S1′ subsite in a manner similar to that of the chlorocinnamic hydroxamate structures (see Figure 4A); this is in striking contrast to the structures of PT-1 and -2, in which Phe369 is rotated away from the subsite and makes no contact with the inhibitors, while Asn368 instead completes the S1′ subsite. The most significant difference between the rodlike structure 2IMA and the structures reported here is the proximity of the Pro69 residue that lies at the tip of the 60/70 loop; in the rodlike structure, Pro69 does not make inhibitor contact, whereas in each of the three structures reported here, Pro69 is drawn >2.5 Å closer to the zinc, creating a portion of the hydrophobic surface of the subsite binding the S3′ arm of the inhibitor and also providing a major interaction with the S1′ arm. Table 3 gives a comparison of key residue positions in these subsites.

The S2′ and S3′ subsites from the $SNAP\text{-}25_{197-202}$-bound BoNT/A LC structure are primarily formed by residues Arg363 and Tyr366.[8] Superposition with the $SNAP\text{-}25_{197-202}$ peptide-bound structure shows that the S3′ arms of the compounds in this study roughly coincide with the P2′ and P3′ residues (Figure S3 of the Supporting Information). However, the S3′ arms of our inhibitors are stacked against the 60/70 loop instead of Arg363

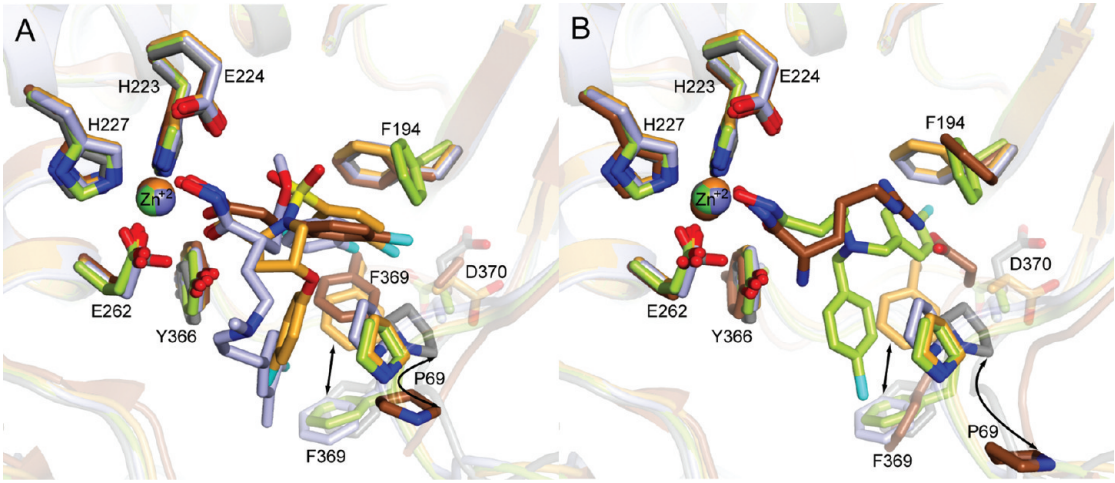

Figure 4. Structural comparison with previously published hydroxamate inhibitors. (A) Structural alignment of BoNT/A LC structures complexed with PT-2 (blue) and PT-3 (orange) and the rodlike 2,4-dichlorocinnamic hydroxamate inhibitor from PDB entry 2IMA (brown).[28] The unliganded BoNT/A LC structure (gray) and PT-1-complexed BoNT/A LC (green; inhibitor omitted for the sake of clarity) structures are also superimposed to highlight the induced-fit structural changes. (B) Structural alignment of BoNT/A LC structures complexed with PT-1 (green) and the rodlike L-arginine hydroxamate inhibitor from PDB entry 2IMB (brown).[28] The unliganded BoNT/A LC structure (gray) and PT-2- and PT-3-complexed BoNT/A LC (blue and orange, respectively; inhibitors omitted for the sake of clarity) structures are also superimposed to highlight the induced-fit structural changes.

and Tyr366. In the PT-2 structure, the methyl ether substituent lies in a subsite that is adjacent to the zinc on the prime side of the active site but bears little relation to the S1′ subsite occupied by Arg198 in the SNAP-25$_{197-202}$ peptide-bound structure. In the structures reported here, as in the other hydrophobic ligand structures,[28] the displacement of Asp370 creates new prime side subsites that are significantly altered from the S1′ binding site of the native substrate.

DISCUSSION

Given the exquisite potency of BoNT/A and the resulting difficulty of inhibiting the activity of the LC sufficiently to provide therapeutic benefit, the discovery and optimization of LC inhibitors as therapeutics are extremely challenging. A more complete understanding of the interactions between inhibitors and key residues in the active site is needed to meet this challenge. Appreciating the nature and range of flexible rearrangements possible within the binding site region is essential for optimization of the design of therapeutic inhibitors.

The three branched scaffold, hydroxamate-based inhibitors of BoNT/A LC are reported here for the first time. The accompanying cocrystal structures show significant commonality despite significant structural differences in the bridging scaffolds of the inhibitors. As expected, the hydroxamate moieties were observed in a classical binding orientation with respect to the active site zinc, including displacement of a putative activated water molecule by the hydroxamate hydroxyl oxygen atom. The S1′ arms of the branched inhibitors coincide with the P1′ residue of SNAP-25 by binding at the S1′ subsite, and the S3′ arms roughly coincide with the P2′ and P3′ subsites through interaction with a conformationally altered 60/70 loop, thereby creating a previously undescribed S2′ and S3′ subsite.

Significance of 360/370 and 60/70 Loop Flexibility. In silico studies previously predicted that surface loops bordering the active site cleft would undergo conformational changes upon binding inhibitors, the largest of which involved the 60/70 loop.[32] Active site flexibility, as previously noted,[28] indeed plays a role in accommodating variation in the positioning of inhibitor moieties occupying the primary binding subsites that roughly correlate to S1′, S2′, and S3′. While a "switch" of Asp370 in the S1′ subsite with Phe369 has been previously reported in the binding of hydrophobic small molecule inhibitors,[28] the role of Asn368 in forming an S1′ subsite, as in our structures for PT-1 and PT-2, has not been previously described. The structures presented here represent a "compact" position of the 60/70 loop in which the C$_\alpha$ atom of Pro69 is 2.6−7.1 Å closer to the active site zinc than in any previously reported BoNT/A LC crystal structures (including small molecule-bound, peptide-bound, unliganded, and holotoxin structures). This orientation of the 60/70 loop creates a compact binding site that tightly surrounds the S1′ *p*-chloro- or *p*-fluorobenzyl arm of each inhibitor in the S1′ subsite. The hydrophobic contacts between Pro69 and the aromatic substituent on the S3′ arm of each inhibitor are likely to provide the energetic impetus for the observed movement of the 60/70 loop. Differences in the position of the 60/70 loop as well as a key hydrophobic S1′ subsite residue, Phe369, are likely to play a large role in the binding of disparate inhibitor classes (e.g., the rodlike hydroxamate reported in PDB entry 2IMA). It is interesting to note that analogues of PT-1, PT-2, and PT-3 that lack a substituent in this arm display no inhibition of BoNT/A LC (unpublished observations). Finally, the 60/70 loop is observed to pack closely against the C-terminal region of residues 415−424 in the holotoxin structure (PDB entry 3BTA; Figure S4 of the Supporting Information). It has been noted that K_i values for small molecule inhibitors can vary significantly when tested in vitro against BoNT/A LC constructs with different C-terminal truncations;[30] the importance of the 60/70 loop position and its interaction with the C-terminal LC region is likely to be at least partially responsible for this observation.

We suspect that binding site flexibility due to mobility of the 60/70 loop and the interplay of residue switching in the 360/370 loop (Asp370-Phe369-Asn368) may be responsible for the difficulties observed by many groups in using structure−activity relationship (SAR) data to guide the synthesis of more potent analogues. The structural insights gained from the analysis of these

cocrystal structures are currently being used in concert with SAR data to improve the design of the next generations of BoNT/A LC inhibitors, which will be reported in due course. While the development of small molecule BoNT inhibitors as intraneuronal therapeutics remains a crucial unmet need, progress toward defining the flexible active site pharmacophore through structure-based drug design is bringing us closer to that goal.

■ ASSOCIATED CONTENT

Supporting Information. Additional figures showing a structural comparison of the active site pockets between BoNT/A LC and thermolysin, electron density maps of the inhibitor-bound and unliganded active site pockets, structural comparison with the SNAP-25 peptide from PDB entry 3DDA, and 60/70 loop proximity with the LC C-terminus. This material is available free of charge via the Internet at http://pubs.acs.org.

■ AUTHOR INFORMATION

Corresponding Author

*The Scripps Research Institute, 10550 N. Torrey Pines Rd., GAC-1200, La Jolla, CA 92037. Telephone: (858) 784-9416. Fax: (858) 784-9483. E-mail: stevens@scripps.edu.

Funding Sources

This work was partially supported by the Pacific Southwest Regional Center of Excellence (U54 AI065359, R.C.S.), National Institute of Allergy and Infectious Diseases SBIR phase I Grant R43 AI069637 (S.O.), and U.S. Department of Defense Contract W81XWH-09-C-0091 (S.O.). The U.S. Army Medical Research Acquisition Activity (820 Chandler St., Fort Detrick. MD 21702-5014) was the awarding and administering acquisition office.

■ ACKNOWLEDGMENT

We thank Jeffrey Velasquez for help with the BoNT/A LC cloning, Angela Walker and Enrique Abola for critical review of the manuscript, and Ms. Linda McKasson for analytical assistance. We also thank the staff of SSRL beamline 11.1 and ALS beamlines 4.2.2 and 12.3.1 for assistance.

■ ABBREVIATIONS

BoNT, botulinum neurotoxin; BoNT/A, botulinum neurotoxin serotype A; BoNT/A LC, botulinum neurotoxin serotype A light chain residues 1−424; SNARE, soluble *N*-ethylmaleimide sensitive factor attachment protein receptor; SNAP-25, 25000 Da synaptosome-associated protein; SNAP-25$_{141-204}$, SNAP-25 peptide residues 141−204; SNAP-25$_{197-202}$, SNAP-25 peptide residues 197−202; rmsd, root-mean-square deviation; 60/70 loop, BoNT/A LC residues 61−79; PT-1, PanThera compound 1; PT-2, PanThera compound 2; PT-3, PanThera compound 3; PDB, Protein Data Bank.

■ REFERENCES

(1) Gill, D. M. (1982) Bacterial toxins: A table of lethal amounts. *Microbiol. Rev. 46*, 86–94.

(2) Rossetto, O., Morbiato, L., Caccin, P., Rigoni, M., and Montecucco, C. (2006) Presynaptic enzymatic neurotoxins. *J. Neurochem. 97*, 1534–1545.

(3) Rossetto, O., and Montecucco, C. (2008) Presynaptic neurotoxins with enzymatic activities. *Handb. Exp. Pharmacol.* 129–170.

(4) Lacy, D. B., Tepp, W., Cohen, A. C., DasGupta, B. R., and Stevens, R. C. (1998) Crystal structure of botulinum neurotoxin type A and implications for toxicity. *Nat. Struct. Biol. 5*, 898–902.

(5) Chen, S., and Barbieri, J. T. (2006) Unique substrate recognition by botulinum neurotoxins serotypes A and E. *J. Biol. Chem. 281*, 10906–10911.

(6) Vaidyanathan, V. V., Yoshino, K., Jahnz, M., Dorries, C., Bade, S., Nauenburg, S., Niemann, H., and Binz, T. (1999) Proteolysis of SNAP-25 isoforms by botulinum neurotoxin types A, C, and E: Domains and amino acid residues controlling the formation of enzyme-substrate complexes and cleavage. *J. Neurochem. 72*, 327–337.

(7) Breidenbach, M. A., and Brunger, A. T. (2004) Substrate recognition strategy for botulinum neurotoxin serotype A. *Nature 432*, 925–929.

(8) Kumaran, D., Rawat, R., Ahmed, S. A., and Swaminathan, S. (2008) Substrate binding mode and its implication on drug design for botulinum neurotoxin A. *PLoS Pathog. 4*, e1000165.

(9) Brunger, A. T., Jin, R., and Breidenbach, M. A. (2008) Highly specific interactions between botulinum neurotoxins and synaptic vesicle proteins. *Cell. Mol. Life Sci. 65*, 2296–2306.

(10) Dolly, J. O., and Aoki, K. R. (2006) The structure and mode of action of different botulinum toxins. *Eur. J. Neurol. 13* (Suppl. 4), 1–9.

(11) Poulain, B., Popoff, M. R., and Molgó, J. (2008) How do the Botulinum Neurotoxins block neurotransmitter release: From botulism to the molecular mechanism of action. *Botulinum J. 1*, 73.

(12) Singh, B. R. (2000) Intimate details of the most poisonous poison. *Nat. Struct. Biol. 7*, 617–619.

(13) Willis, B., Eubanks, L. M., Dickerson, T. J., and Janda, K. D. (2008) The strange case of the botulinum neurotoxin: Using chemistry and biology to modulate the most deadly poison. *Angew. Chem., Int. Ed. 47*, 8360–8379.

(14) Holm, L., and Rosenstrom, P. (2010) Dali server: Conservation mapping in 3D. *Nucleic Acids Res. 38* (Suppl.), W545–W549.

(15) Pang, Y. P., Vummenthala, A., Mishra, R. K., Park, J. G., Wang, S., Davis, J., Millard, C. B., and Schmidt, J. J. (2009) Potent new small-molecule inhibitor of botulinum neurotoxin serotype A endopeptidase developed by synthesis-based computer-aided molecular design. *PLoS One 4*, e7730.

(16) Stowe, G. N., Silhar, P., Hixon, M. S., Silvaggi, N. R., Allen, K. N., Moe, S. T., Jacobson, A. R., Barbieri, J. T., and Janda, K. D. (2010) Chirality holds the key for potent inhibition of the botulinum neurotoxin serotype a protease. *Org. Lett. 12*, 756–759.

(17) Moe, S. T., Thompson, A. B., Smith, G. M., Fredenburg, R. A., Stein, R. L., and Jacobson, A. R. (2009) Botulinum neurotoxin serotype A inhibitors: Small-molecule mercaptoacetamide analogs. *Bioorg. Med. Chem. 17*, 3072–3079.

(18) Lai, H., Feng, M., Roxas-Duncan, V., Dakshanamurthy, S., Smith, L. A., and Yang, D. C. (2009) Quinolinol and peptide inhibitors of zinc protease in botulinum neurotoxin A: Effects of zinc ion and peptides on inhibition. *Arch. Biochem. Biophys. 491*, 75–84.

(19) Burnett, J. C., Wang, C., Nuss, J. E., Nguyen, T. L., Hermone, A. R., Schmidt, J. J., Gussio, R., Wipf, P., and Bavari, S. (2009) Pharmacophore-guided lead optimization: The rational design of a non-zinc coordinating, sub-micromolar inhibitor of the botulinum neurotoxin serotype a metalloprotease. *Bioorg. Med. Chem. Lett. 19*, 5811–5813.

(20) Otwinowski, Z., and Minor, W. (1997) Processing of X-ray Diffraction Data Collected in Oscillation Mode. *Methods Enzymol. 276*, 19.

(21) McCoy, A. J., Grosse-Kunstleve, R. W., Adams, P. D., Winn, M. D., Storoni, L. C., and Read, R. J. (2007) Phaser crystallographic software. *J. Appl. Crystallogr. 40*, 658–674.

(22) Emsley, P., Lohkamp, B., Scott, W. G., and Cowtan, K. (2010) Features and development of Coot. *Acta Crystallogr. D 66*, 486–501.

(23) Adams, P. D., Afonine, P. V., Bunkoczi, G., Chen, V. B., Davis, I. W., Echols, N., Headd, J. J., Hung, L. W., Kapral, G. J., Grosse-Kunstleve, R. W., McCoy, A. J., Moriarty, N. W., Oeffner, R., Read, R. J., Richardson, D. C., Richardson, J. S., Terwilliger, T. C., and Zwart, P. H. (2010) PHENIX: A

comprehensive Python-based system for macromolecular structure solution. *Acta Crystallogr. D 66*, 213–221.

(24) Bricogne, G. B. E., Brandl, M., Flensburg, C., Keller, P., Paciorek, W., Roversi, P., Smart, O. S., Vonrhein, C., and Womack, T. O. (2009) *BUSTER*, version 2.8.0, Global Phasing Ltd., Cambridge, U.K.

(25) Painter, J., and Merritt, E. A. (2006) Optimal description of a protein structure in terms of multiple groups undergoing TLS motion. *Acta Crystallogr. D 62*, 439–450.

(26) Johnson, A. T., and Kim, S. (2010) Hydroxamic acid derivatives of 4-phenyl 4-hydroxy, 4-phenyl 4-alkoxy and 4-phenyl 4-arylalkoxy butyric acid useful as therapeutic agents for treating anthrax poisoning. U.S. Patent 2010/0286125 A1.

(27) Lovell, S. C., Word, J. M., Richardson, J. S., and Richardson, D. C. (2000) The penultimate rotamer library. *Proteins 40*, 389–408.

(28) Silvaggi, N. R., Boldt, G. E., Hixon, M. S., Kennedy, J. P., Tzipori, S., Janda, K. D., and Allen, K. N. (2007) Structures of *Clostridium botulinum* Neurotoxin Serotype A Light Chain complexed with small-molecule inhibitors highlight active-site flexibility. *Chem. Biol. 14*, 533–542.

(29) Zuniga, J. E., Schmidt, J. J., Fenn, T., Burnett, J. C., Arac, D., Gussio, R., Stafford, R. G., Badie, S. S., Bavari, S., and Brunger, A. T. (2008) A potent peptidomimetic inhibitor of botulinum neurotoxin serotype A has a very different conformation than SNAP-25 substrate. *Structure 16*, 1588–1597.

(30) Burnett, J. C., Ruthel, G., Stegmann, C. M., Panchal, R. G., Nguyen, T. L., Hermone, A. R., Stafford, R. G., Lane, D. J., Kenny, T. A., McGrath, C. F., Wipf, P., Stahl, A. M., Schmidt, J. J., Gussio, R., Brunger, A. T., and Bavari, S. (2007) Inhibition of metalloprotease botulinum serotype A from a pseudo-peptide binding mode to a small molecule that is active in primary neurons. *J. Biol. Chem. 282*, 5004–5014.

(31) Kumaran, D., Rawat, R., Ludivico, M. L., Ahmed, S. A., and Swaminathan, S. (2008) Structure- and substrate-based inhibitor design for *Clostridium botulinum* neurotoxin serotype A. *J. Biol. Chem. 283*, 18883–18891.

(32) Burnett, J. C., Schmidt, J. J., McGrath, C. F., Nguyen, T. L., Hermone, A. R., Panchal, R. G., Vennerstrom, J. L., Kodukula, K., Zaharevitz, D. W., Gussio, R., and Bavari, S. (2005) Conformational sampling of the botulinum neurotoxin serotype A light chain: Implications for inhibitor binding. *Bioorg. Med. Chem. 13*, 333–341.